

## Three-parameter AVO inversion with PP and PS data using offset binning

Faranak Mahmoudian and Gary F. Margrave

### ABSTRACT

We have investigated a method of inverting amplitudes of both PP and converted PS prestack data to three parameters — P- and S-wave impedance, plus density. Results from 3-parameter joint inversion are compared with those from 2-parameter joint inversion, which uses only P- and S-wave impedance data. The inversion program performs an AVO inversion using a singular value decomposition (SVD) method. The advantage of the SVD method over the more commonly used least-squares method lies in working with matrices that are either singular or else numerically very close to singular. To investigate the contribution of incorporating both PP and PS data in joint inversion, 3-parameter joint-inversion results are compared to those from PP- and PS-only inversions. To reduce the computation cost of prestack migration (used for improving lateral resolution and correlating PP and PS data in depth), the input datasets are arranged in limited-offset stack sections. Using only a small number of limited-offset stack traces as input to the inversion program produces results as good as using all offset traces.

### INTRODUCTION

The main objective in interpreting seismic data is the extraction of information most related to lithology and/or fluid content of rocks being imaged. The quality most closely related to seismic trace amplitudes — and that which best characterizes rock properties — is elastic impedance, which can be extracted from seismic data. Theoretical knowledge about the variation of reflectivity with offset derived from Zoeppritz equations can be used to estimate impedances. Since the Zoeppritz equations are highly nonlinear with respect to velocities and density, many approximations have been made in order to linearize them. Aki and Richards (1980) assumed small, welded-layer contrasts and simplified the equations. The Aki and Richards linear approximations for PP and PS reflection coefficients,  $R_{PP}$  and  $R_{PS}$ , can be reformulated as function of density and P-wave and S-wave impedance (Larsen 1999), i.e.,  $I = \alpha\rho(\Delta I / I = \Delta\alpha / \alpha + \Delta\rho / \rho)$  and  $J = \beta\rho(\Delta J / J = \Delta\beta / \beta + \Delta\rho / \rho)$  as:

$$R_{PP}(\theta) = A(\theta) \frac{\Delta I}{I} + B(\theta) \frac{\Delta J}{J} + C(\theta) \frac{\Delta\rho}{\rho} \quad (1)$$

$$R_{PS}(\theta, \varphi) = E(\theta, \varphi) \frac{\Delta J}{J} + D(\theta, \varphi) \frac{\Delta\rho}{\rho} \quad (2)$$

where,

$$A(\theta) = \frac{(1 + \tan^2 \theta)}{2} \quad (3)$$

$$B(\theta) = -4 \frac{\beta^2}{\alpha^2} \sin^2 \theta \quad (4)$$

$$C(\theta) = -\left( \frac{\tan^2 \theta}{2} - 2 \frac{\beta^2}{\alpha^2} \sin^2 \theta \right) \quad (5)$$

$$D(\theta, \varphi) = \frac{-\alpha \tan \varphi}{2\beta} \left( 1 + 2 \sin^2 \varphi - 2 \frac{\beta}{\alpha} \cos \theta \cos \varphi \right) \quad (6)$$

$$E(\theta, \varphi) = \frac{\alpha \tan \varphi}{\beta} \left( 2 \sin^2 \varphi - 2 \frac{\beta}{\alpha} \cos \theta \cos \varphi \right) \quad (7)$$

where  $\alpha$  is P-wave velocity,  $\beta$  is S-wave velocity, and  $\rho$  is density. The coefficients A, B, C, D, and E are functions of the P-wave incident angle,  $\theta$ , the S-wave reflected angle,  $\varphi$ , and the S- to P-wave velocity ratio.

Using Gardner's relation between density and P-wave velocity, the density reflectivity term ( $\Delta\rho/\rho$ ) can be rewritten as a function of P-wave impedance,  $\Delta\rho/\rho = (0.2)\Delta I/I$ . This assumption reduces the equations (1) and (2) to linear combinations of 2 parameters  $\Delta I/I$  and  $\Delta J/J$ . In this case, inverting equations (1) and (2) to obtain 2 parameters ( $\Delta I/I$  and  $\Delta J/J$ ) is called 2-parameter joint inversion of PP and PS reflection seismic data. Introduced by Stewart (1990) following of the weighted stack scheme of Smith and Gidlow (1987), 2-parameter joint inversion is based on least-squares inversion. Early applications of 2-parameter joint inversion on real data were by Larsen and Margrave (1999), and Zhang and Margrave (2003). The 2-parameter joint-inversion method by least-squares method is fully discussed in Mahmoudian and Margrave (2003).

Here we present an inversion method to invert equations (1) and (2) using a singular value decomposition (SVD) method to obtain 3 parameters —  $\Delta I/I$ ,  $\Delta J/J$ , and  $\Delta\rho/\rho$ . This method is called 3-parameter joint inversion. Additionally, we have done 2-parameter joint inversion, 3-parameter PP inversion (for only PP data), and 2-parameter PS inversion (for only PS data) with the SVD method.

## THEORY

Assuming that the PP and PS reflection data provide estimates of  $R_{PP}$  and  $R_{PS}$  over a range of source-receiver offsets, the Aki and Richards approximations for different offsets at a certain depth can be used to express a linear system of  $2m$  linear equations ( $m$  being number of offsets) with 3 unknowns:

$$\begin{bmatrix} R_{PP1} \\ \vdots \\ R_{PPm} \\ R_{PS1} \\ \vdots \\ R_{PSm} \end{bmatrix}_{2m \times 1} = \begin{bmatrix} A_1 & B_1 & C_1 \\ \vdots & \vdots & \vdots \\ A_m & B_m & C_m \\ 0 & E_1 & D_1 \\ \vdots & \vdots & \vdots \\ 0 & E_m & D_m \end{bmatrix}_{2m \times 3} \begin{bmatrix} \frac{\Delta I}{I} \\ \frac{\Delta J}{J} \\ \frac{\Delta \rho}{\rho} \end{bmatrix}_{3 \times 1}, \quad (8)$$

or equivalently as the matrix equation:

$$y = Ax, \quad (9)$$

where  $y = (R_{PP1} \dots R_{PPm} \ R_{PS1} \dots R_{PSm})^T$  is the reflection data vector. Matrix  $A$  is a  $2m \times 3$  matrix of known coefficients computed by ray-tracing a smoothed background velocity.  $x = (\Delta I / I \ \Delta J / J \ \Delta \rho / \rho)^T$  is the vector of unknown parameters. The AVO inversion problem has now been reduced to solving the matrix equation (8) to obtain the parameters vector  $x$ . Problem (9) may be approached by operating on both sides with an  $(3 \times 2m)$  'inverse' matrix  $H$  and the 'solution', or model, would be,

$$\hat{x} = Hy. \quad (10)$$

The operator  $H$  will be a good inverse if the response of  $A\hat{x}$  fits the reflection data and the uncertainties in  $\hat{x}$  are not too large, i.e.  $var(\hat{x})$  is small (Jackson, 1971). To find the inverse of the non-square matrix  $A$ , the powerful SVD method is used. The same procedure has been taken in PP and PS inversion only.

### SVD ANALYSIS

For  $2m \times 3$  matrix  $A$  (or, in general, for any  $m \times n$  matrix) with the rank  $r$ , there is always a matrix decomposition called a singular value decomposition (SVD) of matrix  $A$ . Singular value decomposition allows the coefficient matrix  $A$  to be expressed as the product of three matrices (Lay, 1996),

$$A = UDV^T \quad (11)$$

The columns of matrix  $U$  are the eigenvectors of the matrix  $AA^T$ , related to the  $r$  nonzero eigenvalues. The columns of matrix  $V$  are the eigenvectors of the matrix  $A^T A$ , related to the  $r$  nonzero eigenvalues. The singular values of the matrix  $A$  are the positive square roots of the eigenvalues of the matrix  $A^T A$ .  $D$  is a diagonal matrix with the non-zero singular values of the matrix  $A$  in the diagonal elements in the form of:

$$D = \begin{bmatrix} \sigma_1 & & 0 \\ & \ddots & \\ 0 & & \sigma_r \end{bmatrix}_{r \times r} \quad (12)$$

$$\sigma_1 \geq \sigma_2 \geq \dots \geq \sigma_r > 0.$$

The SVD of the  $2m \times 3$  matrix  $A$ , always exists due to exist of matrixes  $U$ ,  $V$  and  $D$ . For any arbitrary matrix  $A$ , the matrixes  $A^T A$  and  $AA^T$  are symmetric, which based on linear algebra have real eigenvalues and orthogonal eigenvectors. In this regard by definition the matrices  $U$ ,  $V$  and  $D$  always exist (Lay, 1996).

Since the diagonal entries in matrix  $D$  are nonzero, the pseudo-inverse (also the Lanczos inverse) of matrix  $A$  is defined as (Lay, 1996):

$$H = VD^{-1}U^T \quad (13)$$

$$H = V \left[ \text{diag} \left( \frac{1}{\sigma_j} \right) \right] U^T \quad (14)$$

Defining the matrix  $H$ , some rules from linear algebra is used including the relations  $UU^T = U^T U = I_{2m}$  and  $VV^T = V^T V = I_r$  for orthogonal matrixes  $U$  and  $V$ . With the definition of pseudo- inverse matrix in equation (13) the following equations hold:

$$HAH = H \quad (15)$$

$$AHA = A \quad (16)$$

Now we return to our inversion problem, equation (9). Using the pseudo-inverse of matrix  $A$ , the parameter vector  $\hat{x}$  can be obtained as:

$$Ax = y \text{ or } HA\hat{x} = Hy = HAHy \quad (17)$$

$$\hat{x} = Hy; \quad (18)$$

equivalently,

$$\hat{x} = VD^{-1}U^T y \quad (19)$$

Knowing the matrices  $U$ ,  $V$  and  $D$  from SVD factorization of matrix  $A$ , the pseudo-inverse matrix  $H$  can be constructed. Then the parameter vector  $\hat{x}$  can be achieved from equation (19). Any possible instability in the numerical calculation of  $\hat{x}$  is identified in matrix  $D$ , because the only thing that can go wrong with using SVD is when inverting a matrix that has some zero or very small singular value like  $\sigma_j$ . As in equation (14), the value of  $(1/\sigma_j)$  is dominated by a round-off error and therefore unknowable. In such cases, we can simply replace  $(1/\sigma_j)$  by zero (Press et al., 1992, and Wiggins, 1971). It may seem paradoxical that this can be so, since zeroing a singular value corresponds to throwing away one linear combination of the set of equations that we are trying to solve. Answering this, Press et al., (1992) state that “*the resolution of the paradox is that we are*

throwing away precisely a combination of equations that is so corrupted by round-off errors as to be at best useless.”

Therefore if the singular values of matrix  $A$  are extremely small, round-off errors are almost inevitable, but an error analysis is aided by knowing the entries in  $D$  and  $V$ . Calculating the  $\hat{x}$  error, the  $var(\hat{x})$  is calculated as:

$$var(\hat{x}_k) = \sum_{i=1}^{2m} H_{ki}^2 var(y_i) \quad (20)$$

For statistically independent data with unit variance, using the definition for inverse matrix  $H$  (equation (14)), the  $\hat{x}$  error is (Jackson, 1972),

$$var(\hat{x}_k) = \sum_{j=1}^r \left( \frac{V_{kj}}{\sigma_j} \right)^2 \quad (21)$$

This allows us to examine each model parameter  $\hat{x}_k$  individually. As we mentioned, a sensitive way to control the variance is to construct the inverse  $H$  out of only those eigenvectors corresponding to large enough eigenvalues. In our model examples, to set a threshold for deciding which eigenvalue is dominating the round-off error, we looked at the condition number of matrix  $A$ . The ratio  $\sigma_1 / \sigma_n$  of the largest and smallest singular values gives the condition number of matrix  $A$ .

## IMPLEMENTATION

The joint inversion program is designed to have PP and PS common image gathers, as well as a velocity-depth model as input. The PP and PS gathers were synthetics created in SYNTH (CREWES MATLAB library). Both gathers were created initially as broadband responses and then convolved with the appropriate wavelet. From our experience, PS data recorded on land has about half the bandwidth of the corresponding PP data. Therefore, the PS synthetics were generated with a different initial wavelet than the PP synthetics. The combination of PP and PS data in an inversion requires that the two data types be correlated in time or depth. We followed a procedure to correlate the PP and PS synthetic sections in depth. At each depth sample, the coefficient matrix (matrix  $A$  in equation (9)), is calculated. Using the SVD factorization of matrix  $A$ , the pseudo-inverse matrix  $H$  in equation (13) is constructed using the routine RINV (CREWES MATLAB library). As a last step, the parameters vector  $\hat{x}$  is calculated from equation (17). The three components of parameters vector  $\hat{x}$  are the estimated  $\Delta I/I$ ,  $\Delta J/J$ , and  $\Delta \rho/\rho$ .

For each depth sample, the estimated reflectivity results, ( $\Delta I/I$ ,  $\Delta J/J$ , and  $\Delta \rho/\rho$ ), were integrated to  $I$ ,  $J$  and  $\rho$  using the band-limited impedance routine (BLIMP) from the CREWES MATLAB library. The BLIMP routine is a simple algorithm for band-limited impedance inversion (Ferguson and Margrave, 1996). To approximate the subsurface impedance using seismic data, it is necessary to account for the band-limited nature of seismic data, especially for low-frequencies (Ferguson and Margrave, 1996). The BLIMP routine uses impedance estimated from logs (or a density model) to provide the missing low-frequency components of the input seismic data. In summary, we inverted PP and PS

amplitudes to  $I$ ,  $J$  and  $\rho$  including the low-frequency component, which significantly improves the inversion results (Mahmoudian and Margrave, 2003).

### 2- and 3-parameter joint inversion

The parameter vector  $\hat{x}$  calculated by 2-parameter joint inversion is consisted of  $\Delta I/I$  and  $\Delta J/J$ . The parameter  $\Delta\rho/\rho$  is calculated using Gardener's rule from  $\Delta I/I$  term as  $\Delta\rho/\rho = (0.2)(\Delta I/I)$ . Extending 2-parameter joint inversion to 3-parameter joint inversion for modelling the same data, helps the response of  $A\hat{x}$  fit the data better by avoiding another approximation for  $\Delta\rho/\rho$  term. Such extension theoretically will result in more accurate estimation for all 3 parameters.

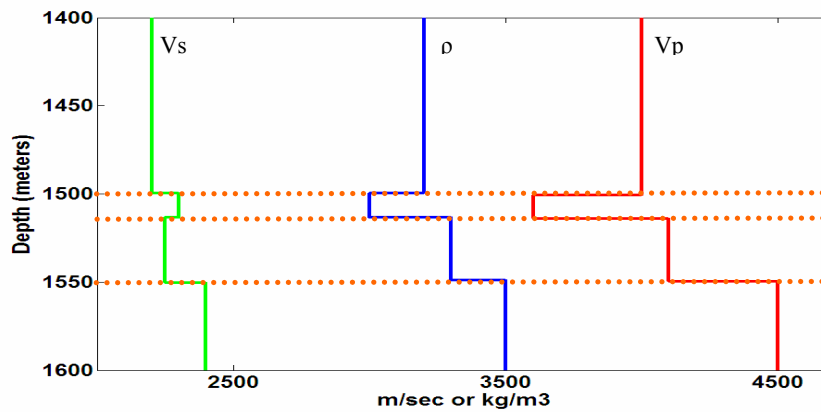


FIG.1. A simple velocity model in depth.

To compare the 3-parameter joint inversion with 2-parameter joint inversion, the inversion results for the sample velocity model of Figure 1 is shown in Figure 2. Note that in 2-parameter joint inversion, the estimated  $\rho$  comes from the estimated  $I$  by using Gardener's rule. In Figure 2, red plots are the inversion results from the 3-parameter joint inversion and green plots are inversion results from the 2-parameter joint inversion, and the blue plots are true value directly calculated from the logs. Note this example obeys Gardener's rule, and it is expected that 2-parameter has also good estimation for  $\Delta\rho/\rho$ .

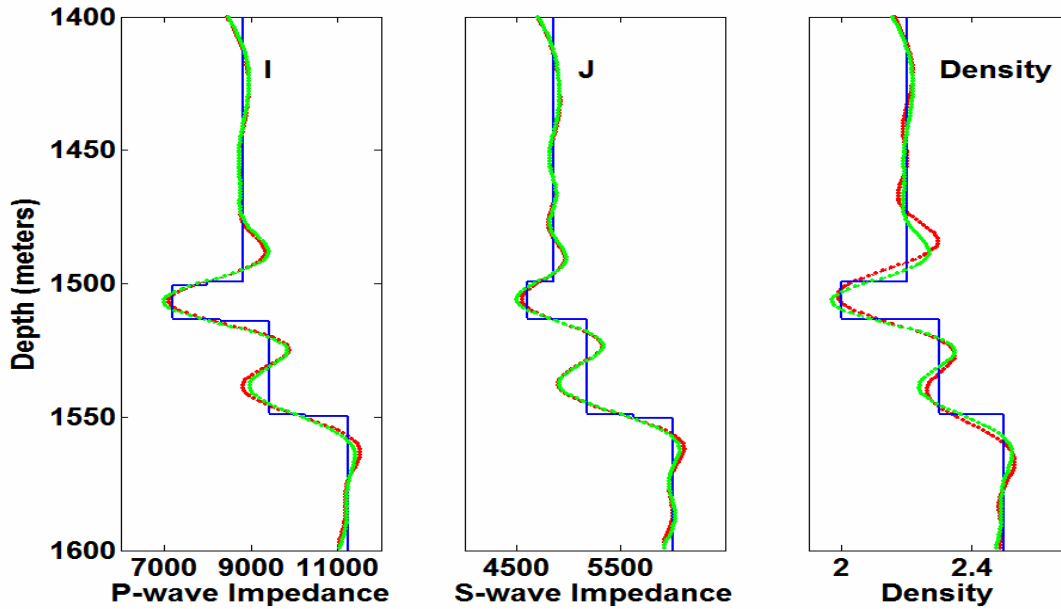


FIG. 2. Comparing the estimated  $I$ ,  $J$  and  $\rho$  from 2-parameter and 3-parameter joint inversions for the sample velocity model in Figure 1. The red line plots the results from 3-parameter joint inversion; the green line plots the results from the 2-parameter joint inversion method, and the blue line plots the true value.

To demonstrate the advantages of 3-parameter joint inversion over 2-parameter joint inversion, the inversion results for the sample velocity model of Figure 3 is shown in Figure 4. Note that, for the velocity model of Figure 3, the density doesn't obey Gardner's rule. Figure 4 clearly shows that 3-parameter joint inversion can estimate density even when density is uncorrelated with P-wave velocity. A careful look at Figure 4 reveals that 2-parameter joint inversion can estimate  $I$  and  $J$  almost as good as 3-parameter joint inversion.

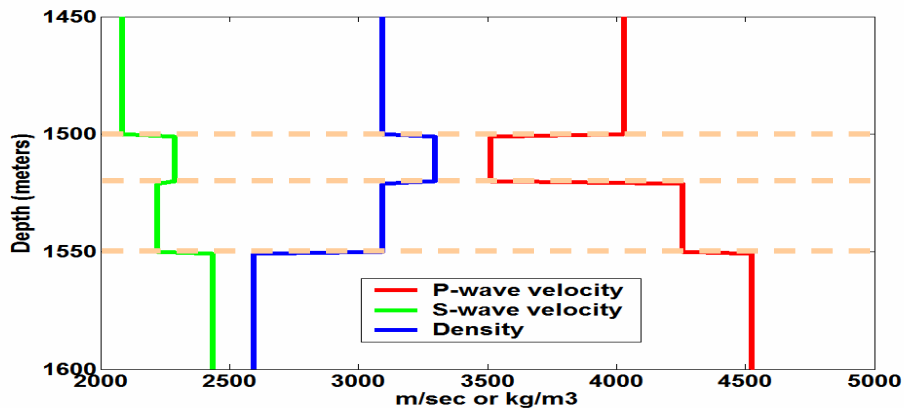


FIG. 3. A simple velocity model in depth.

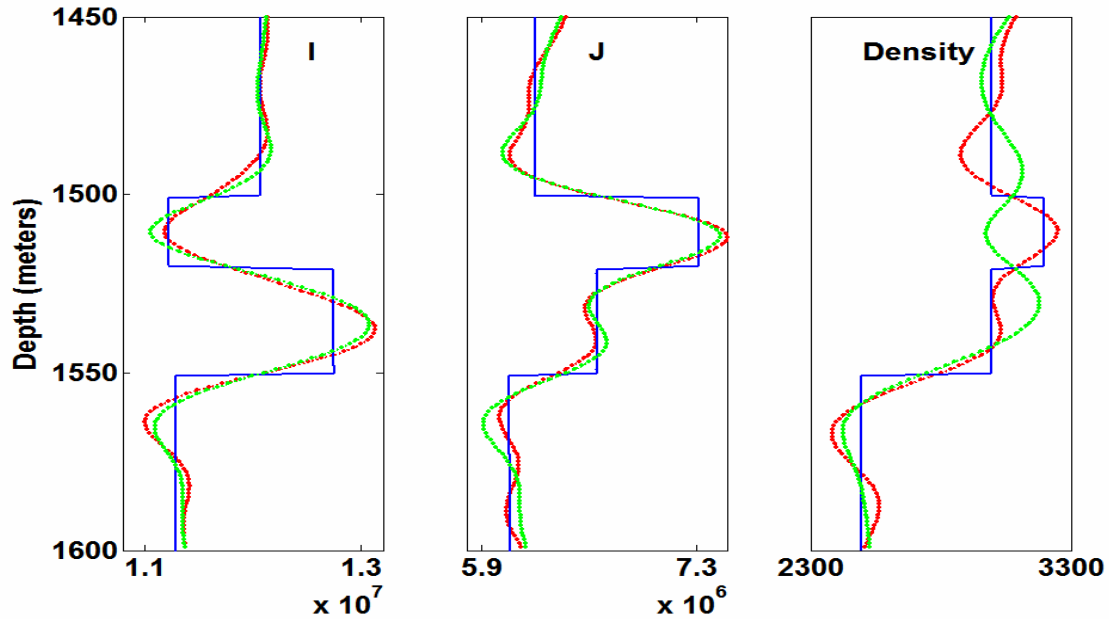


FIG. 4. Comparison of the estimated  $I$ ,  $J$  and  $\rho$  from 2- and 3-parameter joint inversions for the sample velocity model in Figure 3. The red plots display results from 3-parameter joint inversion; the green plots display the inversion results from the 2-parameter joint inversion method, and the blue plots are true values.

### Comparing 3-parameter joint inversion with PP- and PS-only inversions

In this paper, we term the separate inversions of either PP or PS reflection data with the SVD method, PP-only and PS-only inversions, respectively. PP inversion only gives estimations for  $I$ ,  $J$  and  $\rho$  and PS inversion only gives estimations for  $J$  and  $\rho$ . The estimation of  $I$  in PS-only inversion is calculated from the  $\rho$  estimation by Gardener's rule.

The joint inversion, by co-operating more equations due to the addition of PS data (rather than PP inversion only) or PP data (rather than PS inversion only), theoretically results in a more accurate solution. For the sample velocity model in Figure 3, the advantage of joint inversion over PP- or PS-only inversions are shown in Figures 5–10. In Figures 5–10, the red plots display the results from joint inversion; the black plots display the results from PP- or PS-only inversions; the blue plots are true values. For the velocity model example in Figure 3, the input PP and PS synthetics gather to inversion program, is generated with the initial zero-phase wavelets 5-10-80-100 and 3-7-57-70, respectively. With these initial wavelets for the velocity model in Figure 3, the generated PP and PS gather has an identical wave-number bandwidth. In Figures 5 and 6, the estimated results from above three inversions are compared using synthetic noise-free data. Figures 5 and 6 show that joint inversion can estimate  $I$ ,  $J$ , and  $\rho$  better than PP- or PS-only inversions.

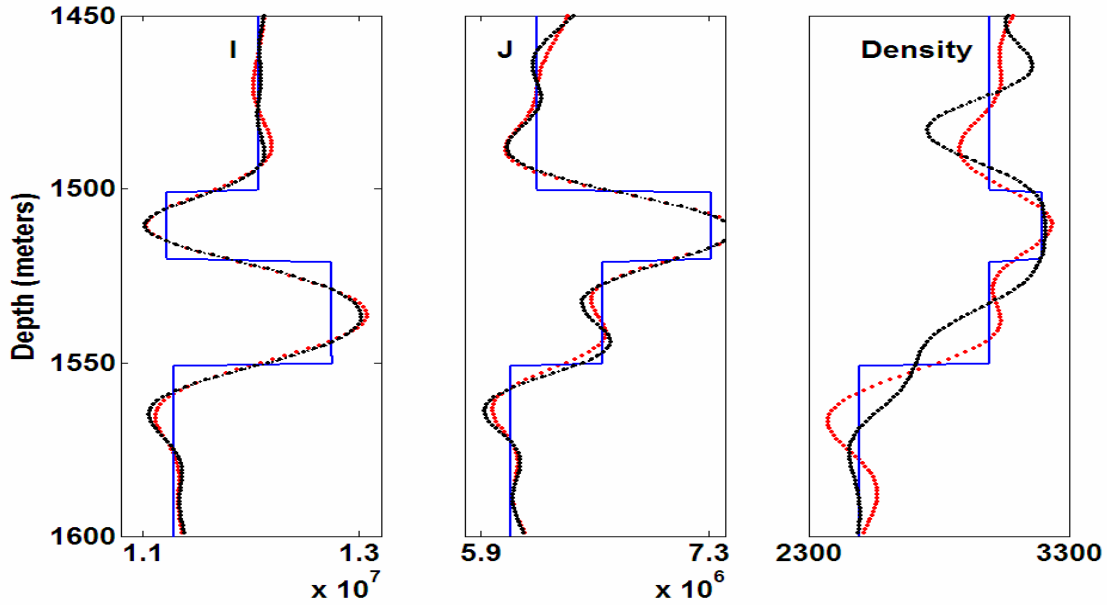


FIG. 5. Comparing the estimated  $I$ ,  $J$  and  $\rho$  from PP-only and joint inversions from noise-free data for the sample velocity model in Figure 3.

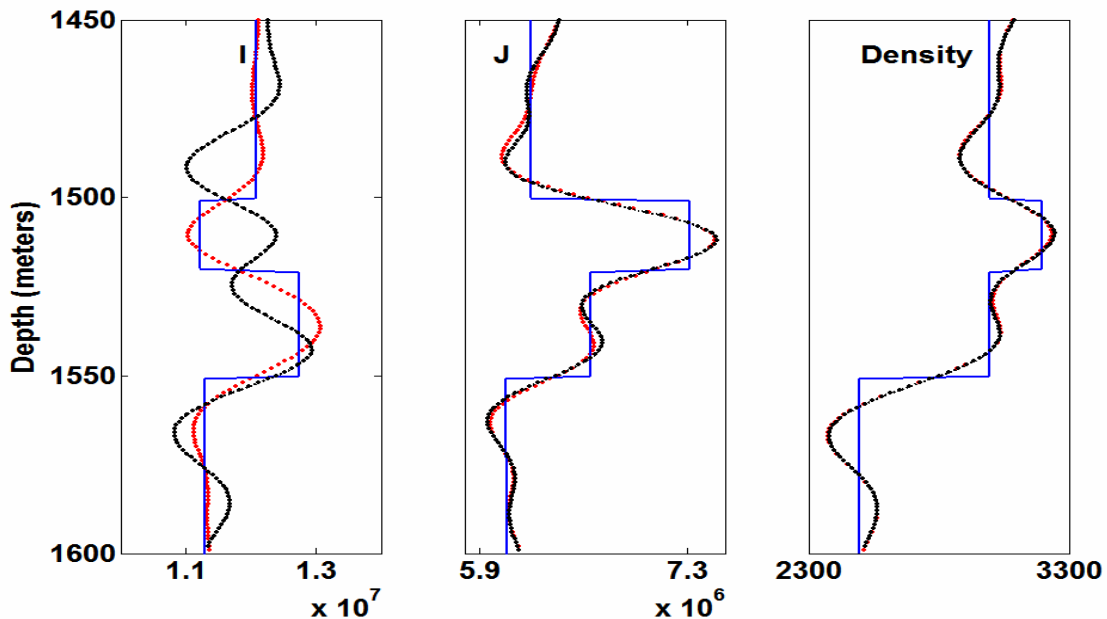


FIG. 6. Comparing the estimated  $I$ ,  $J$  and  $\rho$  from PS-only and joint inversions from noise-free data for the sample velocity model in Figure 3.

Since the joint-inversion method has twice the input data compared to PP or PS inversion only, it is reasonable to assume a corresponding improvement in signal-to-noise is possible (Larsen, 1999). To examine the effect of noise upon inversion accuracy, random noise was added to the synthetic data. Figures 7 and 9 show the inversion results from noisy data with signal-to-noise ratio of 2. This amount of noise is larger than is

typically encountered in real surface seismic data. The inversion results after adding more noise to the data, to reach a signal-to-noise ratio of 1, are shown in Figures 8 and 10. Figures 7–10 show very clearly that the joint inversion method obtains very good results even from very noisy data. Furthermore, Figures 7 and 8 show that the estimations of  $J$  and  $\rho$  from PP-only inversion are highly sensitive to the presence of noise, while the same inversion resulted in a good estimation for  $I$ . Similarly, Figures 9 and 10 show that the estimation of  $I$  from PS-only inversion is highly sensitive to the presence of noise, while providing good estimations for  $J$  and  $\rho$ .

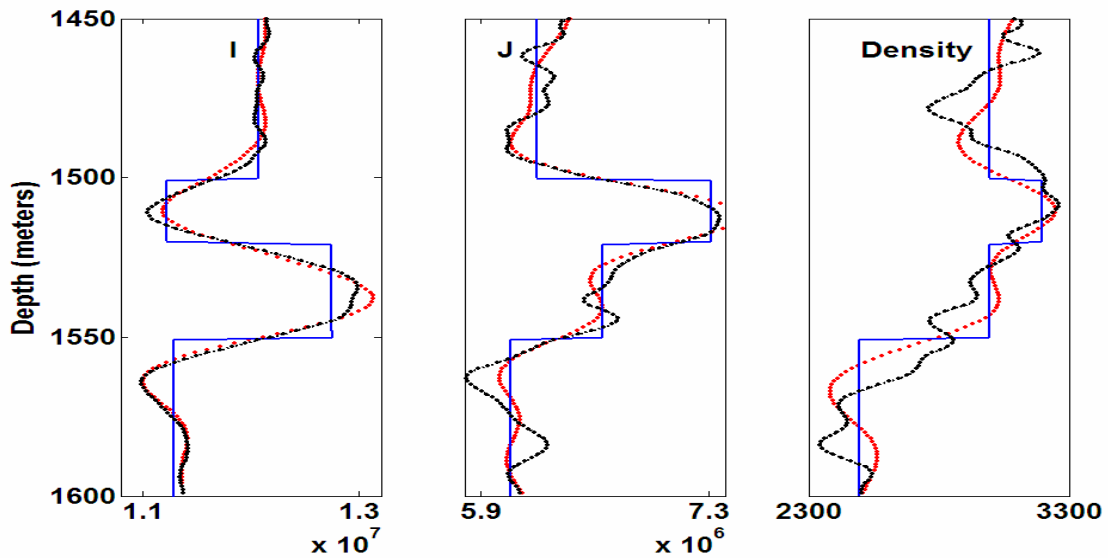


FIG. 7. Comparing the estimated  $I$ ,  $J$  and  $\rho$  from PP-only and joint inversions of noisy data with a signal-to-noise ratio of 2, for the sample velocity model in Figure 3.

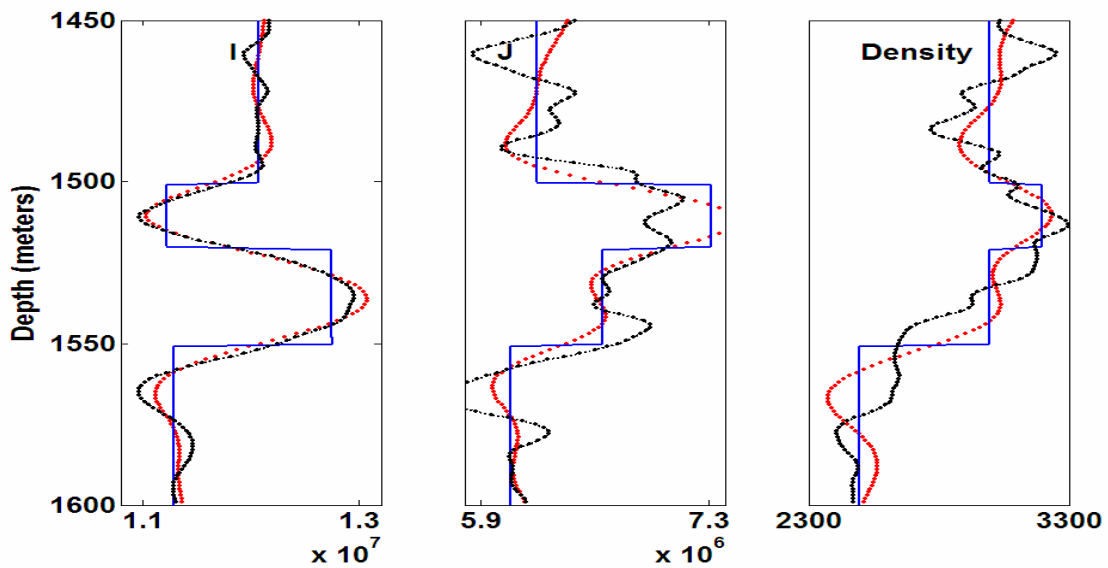


FIG. 8. Comparison of the estimated  $I$ ,  $J$  and  $\rho$  from PP-only and joint inversions of noisy data with a signal-to-noise ratio of 1, for the sample velocity model in Figure 3.

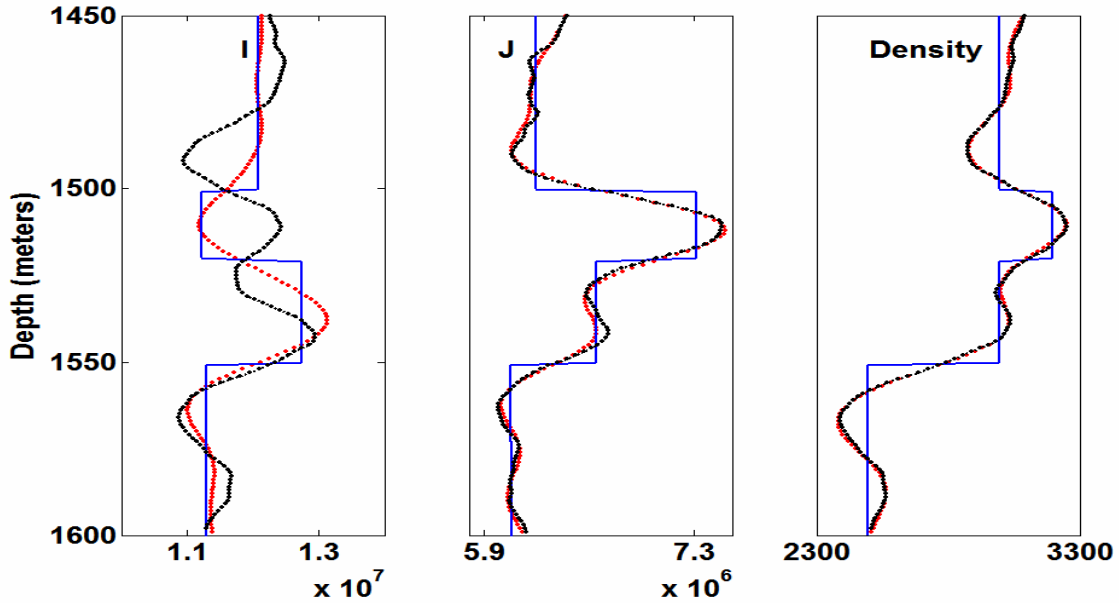


FIG. 9. Comparison of the estimated  $I$ ,  $J$  and  $\rho$  from PS-only and joint inversions of noisy data with signal-to-noise ratio of 2, for the sample velocity model in Figure 3.

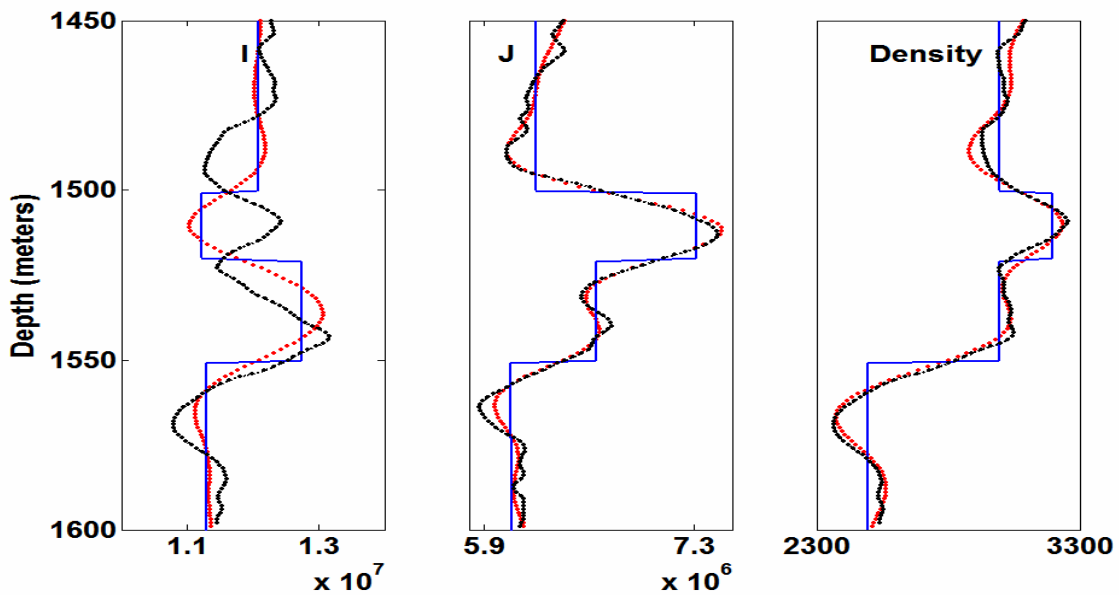


FIG. 10. Comparison of the estimated  $I$ ,  $J$  and  $\rho$  from PS-only and joint inversions of noisy data with a signal-to-noise ratio of 1, for the sample velocity model in Figure 3.

### Inversion of a real log example

In this section, the inversion results for the real velocity model in Figure 11 are examined. The velocity model comes from the Blackfoot Field in southeastern Alberta, Canada, owned and operated by EnCana. The PP and PS synthetics were generated with

different input wavelets. A zero-phase (Butterworth) wavelet 5-10-80-100 was used for PP synthetics, and another zero-phase wavelet, 3-7-57-70, was used for PS synthetics. Both PP and PS synthetics have the same offset range of 0 to 2000 m.

In this example, the singular values of a matrix of coefficients  $A$  were examined at each sample depth using joint inversion. At 1500 metres, the singular values of coefficient matrix  $A$  are 3.22, 1.29, and 0.25. The condition number of matrix  $A$  at this depth is approximately 0.07, which is not a very small number and there is no need to eliminate any small singular values. The coefficient matrix  $A$  has similar singular values at other depths. At 1500 metres, the errors of  $I$ ,  $J$ , and  $\rho$  are 0.2, 1.29, and 14.4, respectively. The errors at other depths are similar. These errors show that joint inversion can estimate  $I$  more accurately than  $J$  and  $\rho$ . Furthermore, they show that joint inversion can estimate  $J$  more accurately than density. The estimations for  $I$ ,  $J$ , and  $\rho$  obtained by joint inversion for the velocity model in Figure 11 are shown in Figure 12. Figure 12 shows a good estimation for the three parameters  $I$ ,  $J$ , and  $\rho$  from 3-parameter joint inversion.

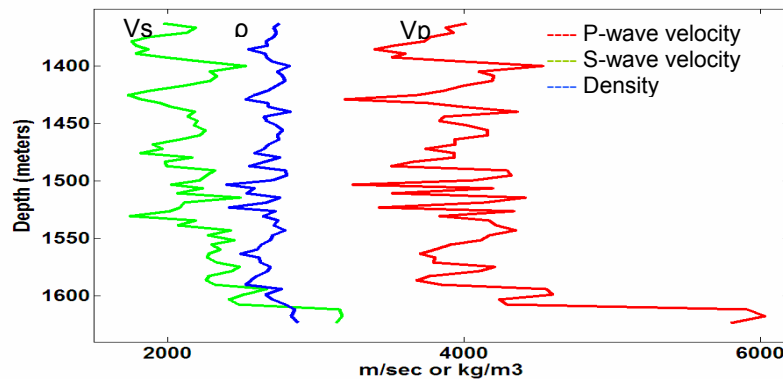


FIG. 11. Real velocity logs from the Blackfoot Field.

The PP-only inversion was done for velocity using SVD method. At 1500 metres, the singular values of coefficient matrix  $A$  are 3.1, 0.5, and 0.08. At this depth, the condition number of matrix  $A$  equals 0.026, which is a large-enough ratio, and means that there is no need to eliminate any small singular values. The coefficient matrix  $A$  has similar singular values for other depths. Therefore, for all sample depths, no singular values were removed. At 1500 metres, the errors of  $I$ ,  $J$ , and  $\rho$  are 0.67, 9.21, and 145 respectively. The estimated results from PP-only inversion and joint inversion are compared in Figure 13. Figure 13 shows that 3-parameter joint inversion can better estimate  $J$  and  $\rho$  than 3-parameter PP-only inversion, although PP-only inversion has very good estimation for  $I$ .

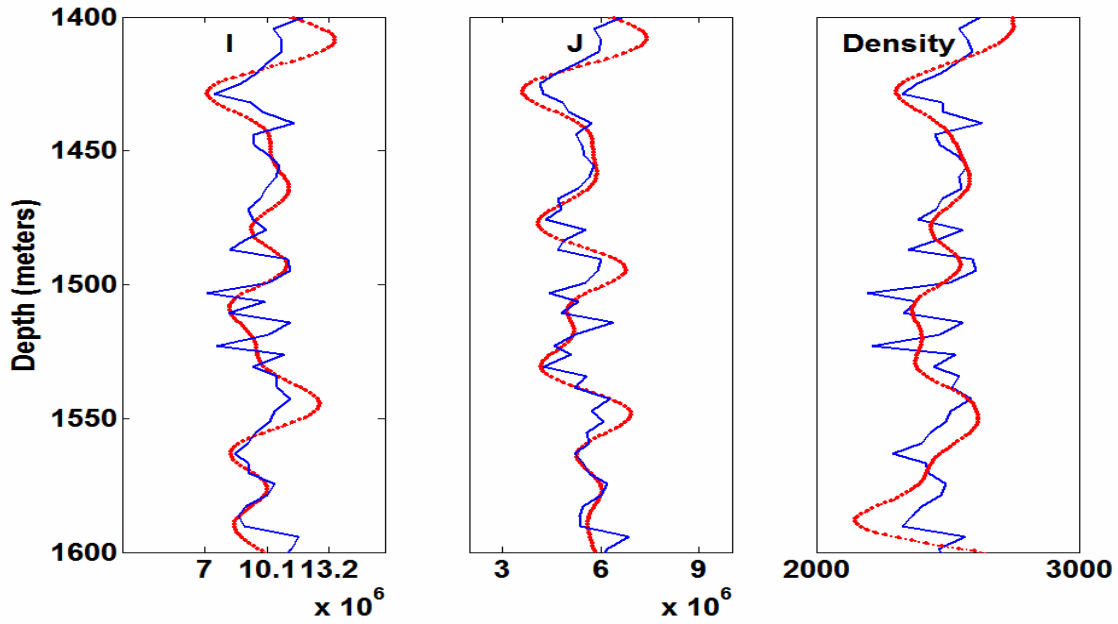


FIG. 12. The estimated  $I$ ,  $J$ , and  $\rho$  from 3-parameter joint inversion for the real velocity model in Figure 11. The red lines plot the joint-inversion results, and the blue lines plot true values.

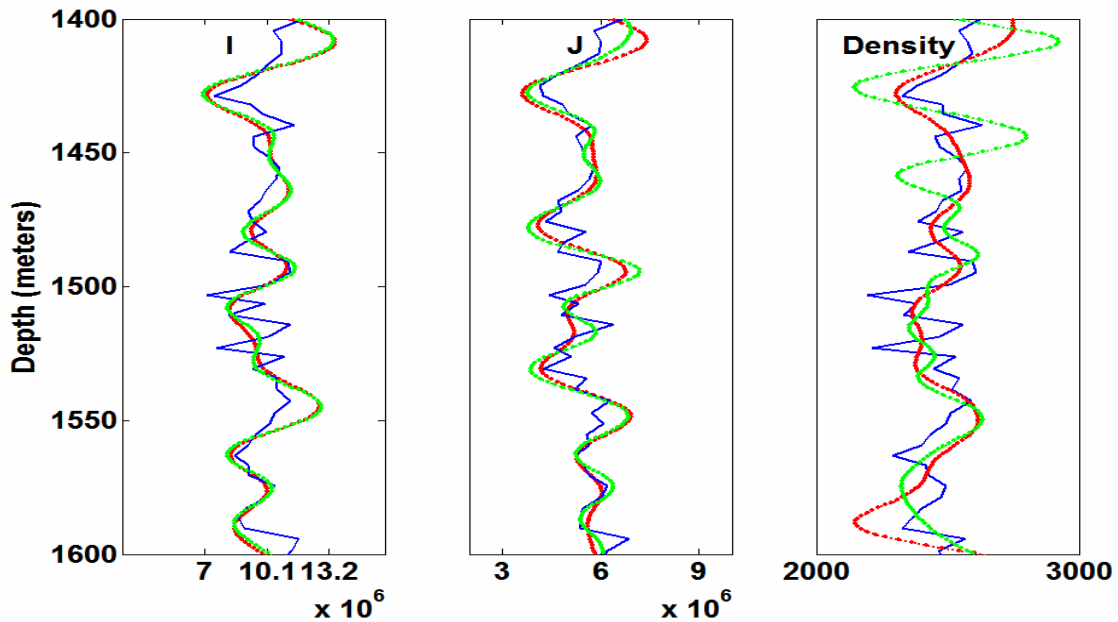


FIG. 13. Comparison of the estimations for  $I$ ,  $J$ , and  $\rho$  from 3-parameter PP-only and joint inversions for the real velocity model in Figure 11. The red lines plot the joint-inversion results; the green lines plot PP-only inversion results; and the blue lines plot true values.

In a similar manner, the PS-only inversion was done for the model in Figure 11. At 1500 metres, the singular values of the coefficient matrix  $A$ , are 1.26, 0.24. Note that the PS-only inversion estimates  $J$  and  $\rho$ , and the estimation of  $I$  is calculated by Gardener's relation. The condition number of matrix  $A$  at this depth is approximately 0.19, which is

large-enough ratio, and means that there is no need to eliminate any small singular values. The coefficient matrix  $A$  has similar singular values for other depths. Therefore, in PS-only inversion, no singular values were removed for all sample depths. At 1500 metres, the errors of  $J$  and  $\rho$  are 1.51 and 16.76, respectively. The estimated results from PS-only and joint inversions are compared in Figure 14. Figure 14 shows that joint inversion can better estimate  $I$ ,  $J$ , and  $\rho$  than PS-only inversion, although PS-only inversion has very good estimation for  $J$  and  $\rho$ .

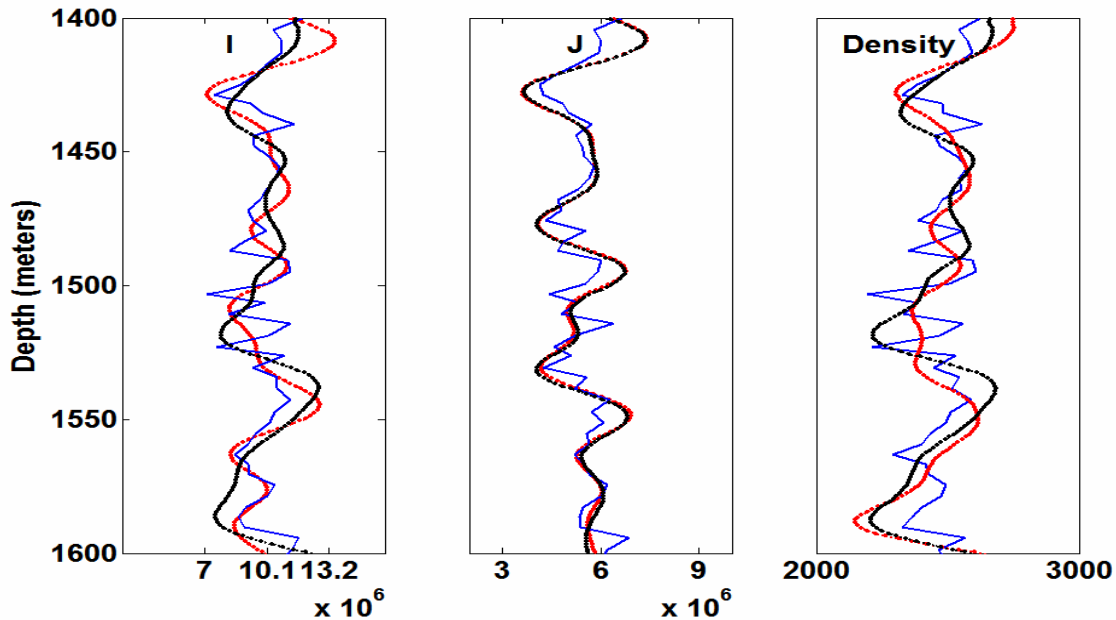


FIG. 14. Comparing the estimated  $I$ ,  $J$ , and  $\rho$  from PS-only and joint inversions for the real velocity model in Figure 11. The red lines plot joint inversion results; the black lines plot PS-only inversion results, and the blue lines plot true values.

To examine the reliability of 3-parameter joint inversion for the velocity model in Figure 11, the input PP and PS synthetics were generated with a broadband initial wavelet. The estimated  $I$ ,  $J$ , and  $\rho$  from joint inversion with non-smoothed input velocity is shown in Figure 15. In Figure 15, the black curve is estimated from joint inversion and the blue curve is the true value from the logs. The difference between estimated  $I$ ,  $J$ , and  $\rho$ , and true values is mainly due to two reasons — using the linear Aki and Richards approximations instead of exact Zoeppritz equations, and using the smoothed velocity model. To examine the impact of smoothing the velocity, the program is run with highly smoothed velocity as input. The estimated  $I$ ,  $J$ , and  $\rho$  from joint inversion with this highly smoothed input velocity is shown in Figure 16. In Figure 16, the red curve is estimated with highly smoothed velocity, the black curve is estimated with non-smoothed velocity, and the blue curve is the true value from the logs. Comparing the black curve and red curve in Figure 16 shows that the joint inversion performs very well with even highly smoothed input velocity for  $I$  and  $J$  estimations, and provides a decent density estimation. Therefore, there is no need to use exact velocity information in applying the joint inversion.

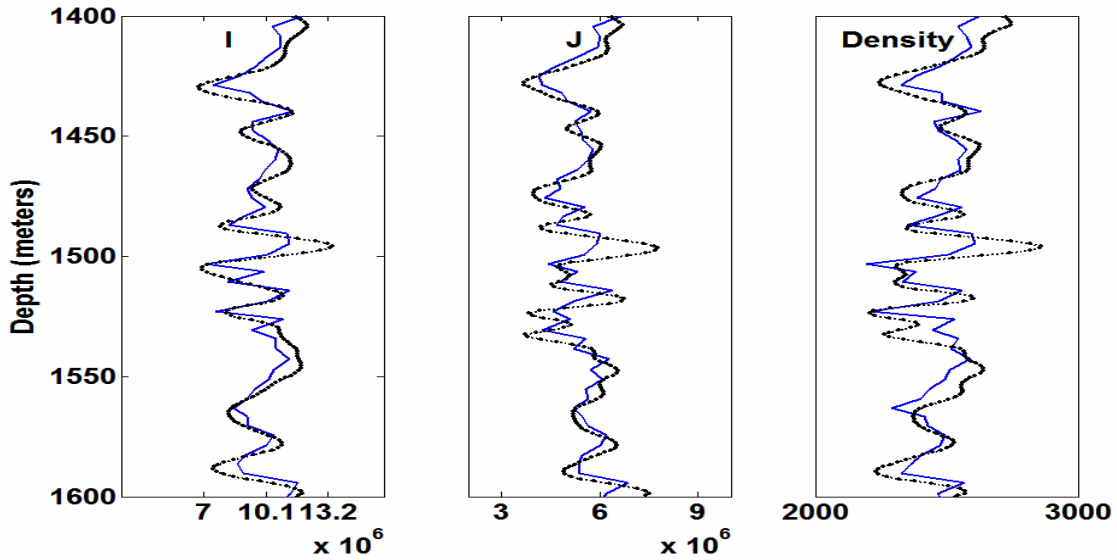


FIG. 15. The estimated  $I$ ,  $J$ , and  $\rho$  of broadband data with non-smoothed velocity from joint inversion for the real velocity model in Figure 11.

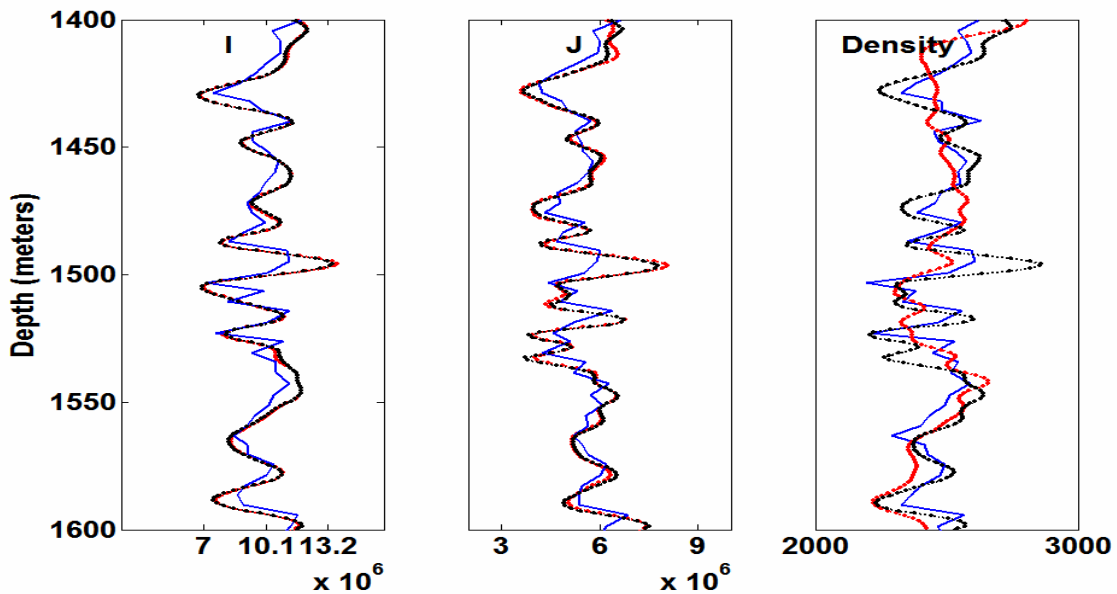


FIG. 16. The estimated  $I$ ,  $J$ , and  $\rho$  from joint inversion for the real velocity model in Figure 11. The red lines plot inversion results with highly smoothed velocity; the black plots display the inversion results with non-smoothed velocity; and the blue plots are true value.

### SVD: the best least-squares solution

The SVD solution of the equations (9), parameters vector  $\hat{x}$  (the estimated  $\Delta I/I$ ,  $\Delta J/J$  and  $\Delta\rho/\rho$ ), is also a least-squares solution (Jackson, 1972, and Lay, 1996). In general, SVD finds the least-squares best compromise solution (Press et al., 1992). The advantage of using SVD over the normal least-squares method is in dealing with matrices that are either singular or else numerically very close to singular. A matrix is called singular

when it has some singular value equal to zero. SVD will diagnose precisely when a matrix is singular and give a useful numerical answer.

To demonstrate this, the 3-parameter joint inversion is applied to a velocity model (Figure 1) using two methods — SVD and least-squares. In this example, the input PP and PS synthetic gathers are generated with an initial zero-phase wavelet 5-10-80-100, and a zero-phase wavelet 5-10-30-40, respectively. At each sample depth, the singular values of the matrix of coefficients  $A$  were examined. At 1500 metres, the singular values of coefficient matrix  $A$  are 3.48, 1.42 and 0.8. At this depth, the condition number of matrix  $A$  is 0.23. The coefficient matrix  $A$  is also similar for other depths. Theoretically, the SVD method is expected to have identical results for inverting a matrix to those from the least-squares method, which are neither singular nor near singular

Figure 17 shows the estimated  $I$ ,  $J$ , and  $\rho$  from the 3-parameter joint inversion program. In this figure, the red lines plot the inversion results using the SVD method, and the green lines plot the results using the least-squares method. As we expected in theory (Figure 2), the identical red and green plots show that the SVD solution is also a least-squares solution.

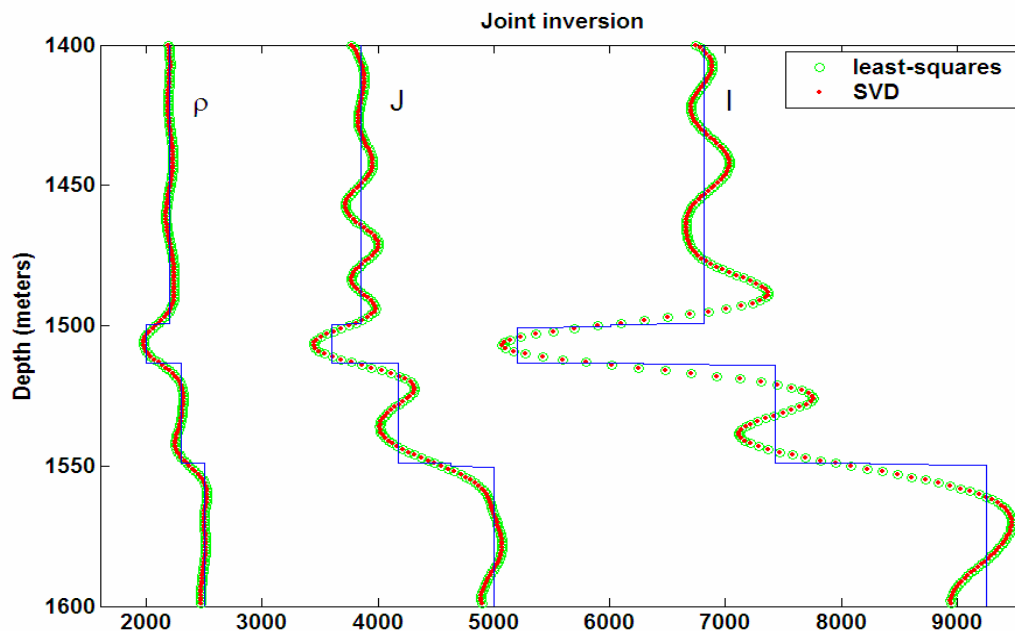


FIG. 17. Comparing the estimated  $I$  and  $J$  and  $\rho$  from 3-parameter joint inversion by SVD and least-squares methods, for the sample velocity model in Figure 1. The red lines plot inversion results using the SVD method, and the green lines plot the inversion results using the least-squares method.

To demonstrate the advantage of using SVD over the common least-squares method, the real velocity model in Figure 11 is used for PP-only inversion. The input PP gather was generated with an initial zero-phase wavelet, 5-10-80-100. At 8400 ft, the singular values of coefficient matrix  $A$  are 1.6633, 0.0078, and  $10^{-6}$ . At this depth, the condition number of matrix  $A$  is approximately  $10^{-7}$ . The coefficient matrix  $A$  has similar singular

values for other depths. To stabilize the inversion, we zeroed the smallest singular value at all depths. The PP-only inversion results with the least-squares and SVD methods are shown in Figures 18 and 19. In Figure 18, the incorrect estimation for  $J$  and very poor estimation for  $\rho$  is clear. Compare this to Figure 19, where the inversion results using the SVD method show very accurate estimations for  $I$ ,  $J$ , and  $\rho$ . Comparing  $I$ ,  $J$ , and  $\rho$  in Figures 18 and 19 is a very good example showing the advantage of using the powerful SVD method over the more common least-squares method.

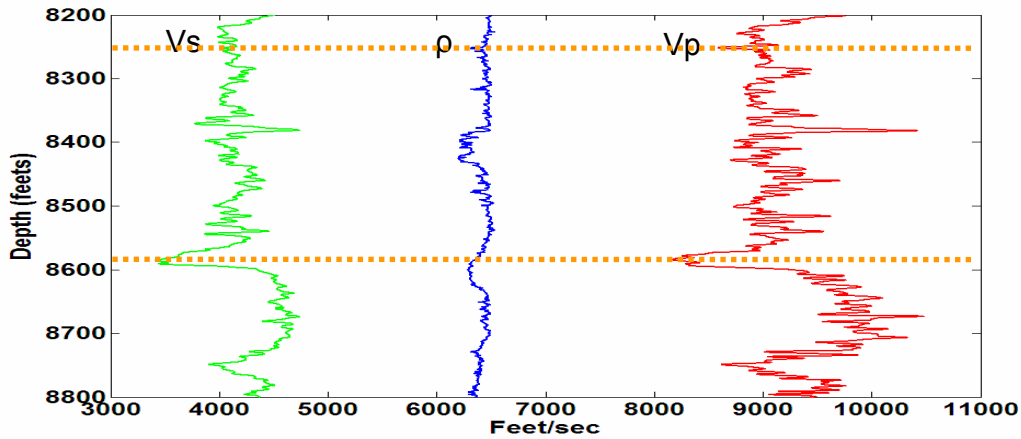


FIG. 18. A real velocity model, with measurements in feet. For greater clarity, the density log was shifted to the right by a constant. The log comes from UNOCAL.

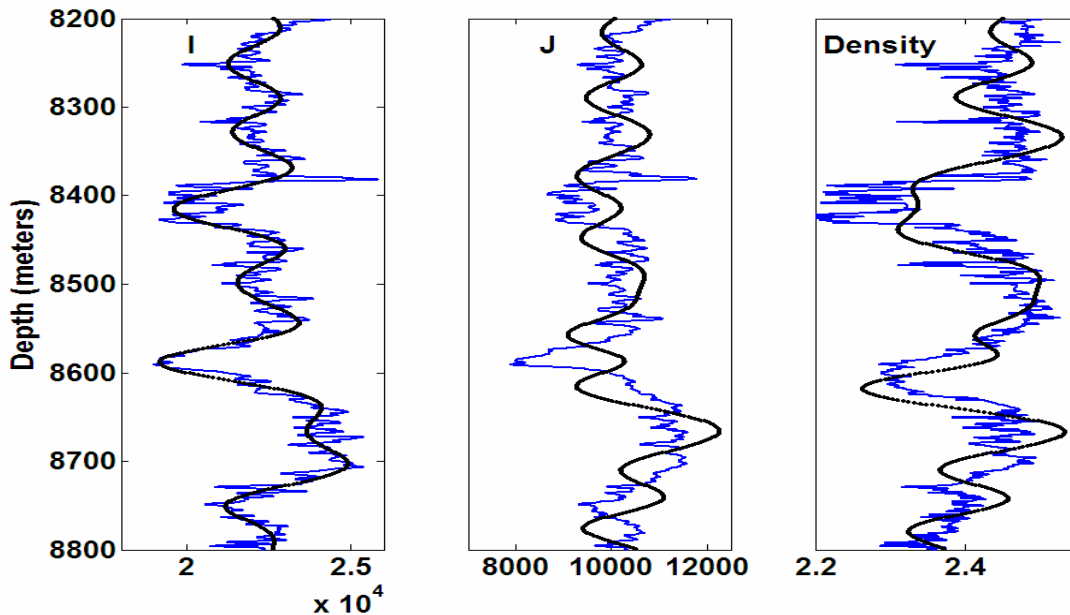


FIG. 19. The estimated  $I$ ,  $J$ , and  $\rho$  from PP-only inversion for the real velocity model in Figure 18. The black lines plot display inversion results using the least-squares method, and the blue lines plot the true values.

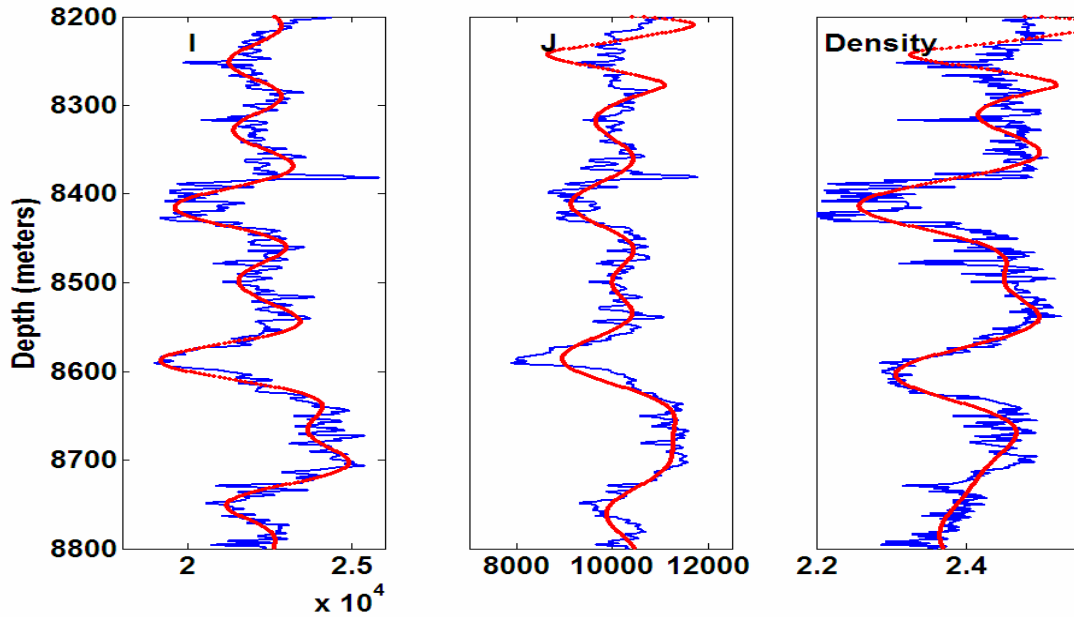


FIG. 20. The estimated  $I$ ,  $J$ , and  $\rho$  from PP-only inversion for the real velocity model in Figure 18. The red lines plot the SVD method inversion results, and the blue lines plot true values.

### Binning size effect on inversion results

Conventional seismic inversion uses a single seismic trace, assumed to be at vertical incidence, for impedance inversion. The joint-inversion algorithm uses several seismic traces which share a common subsurface reflection or conversion point, but which have different angles of incidence (Henley et al., 2002). We first converted the CDP (PP case) and CCP (PS case) gathers to depth, and used these gathers as input to the inversion program. In the case of real datasets, converting to depth requires prestack migration. Prestack migration takes considerable computation time, due to the large number of traces in each gather. Computation cost can be significantly reduced using a more favourable arrangement of raw CDP and CCP gathers. Henley et al. (2002) describes using the limited-offset stack traces from either CDP or CCP gathers as input for the joint-inversion module in ProMAX. Each limited-offset stack trace is the result of stacking NMO-corrected PP or PS traces from a limited range of offsets, and represents the mean offset for traces which were stacked.

For the real log model in Figure 11, a PP and PS gather was created with 21 traces within the offset range of 0–2000 metres with a signal-to-noise ratio of 2, as shown in the topmost plots in Figure 21. The limited-offset stack sections, with 5 non-overlapping bins, are shown in the lower plots in Figure 21 for this PP and PS gather.

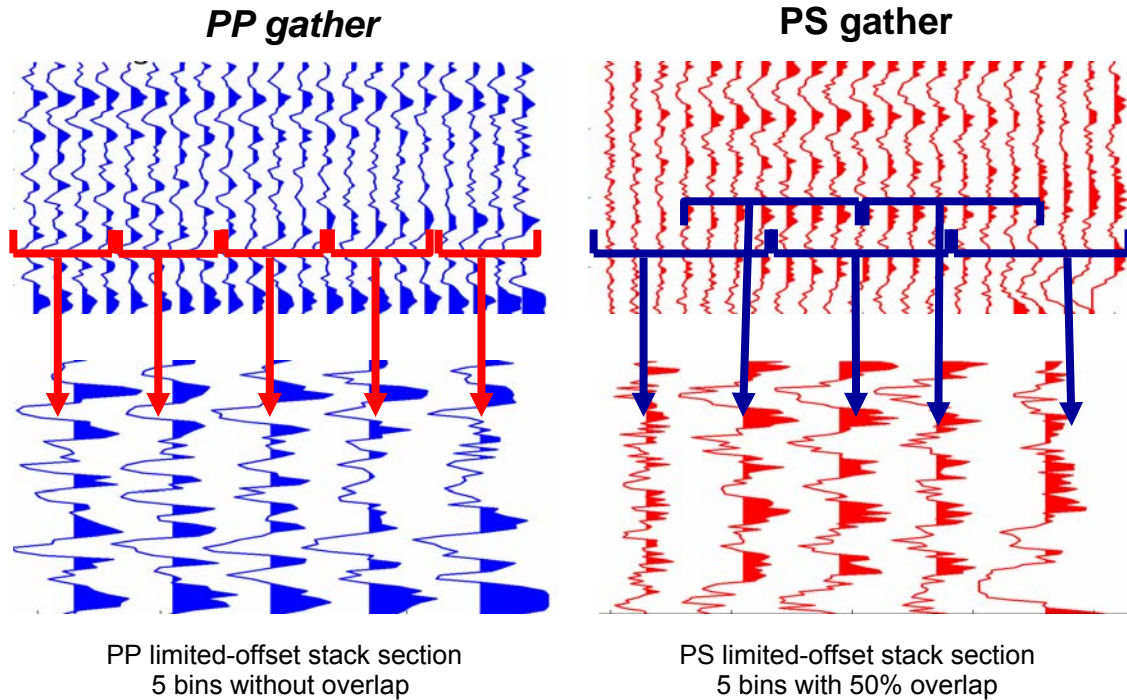


FIG. 21. Top: The PP and PS gather for the real log model in Figure 11. Bottom: The PP limited-stack section with five limited-offset stack traces (5 bins with no overlap) on the left and the PS limited-stack section with five limited-offset stack traces (5 bins with 50% overlap) on the right.

After the limited-offset stack sections were entered into the inversion program, a poststack migration was performed as opposed to a full prestack migration. This method reduces the expense of inversion at the risk of decreasing the accuracy of the result. The number of input limited-offset stack traces is called the binning size. For the real log example in Figure 11, we calculated the RMS error for the  $I$ ,  $J$  and  $\rho$  estimations, to see the impact of binning size on inversion results. These estimations for different bin sizes are compared to the actual values. The RMS error of estimated  $I$ ,  $J$  and  $\rho$  in the zone of interest, between 1400–1500 metres, is shown in Figure (21).

The P- and S-wave impedance, and density estimations from the 3-parameter joint inversion of 3 bins, 5 bins with no overlaps, full-offset traces with no binning, and the actual value are shown in Figure 22. The red lines are inversion results using 3-bin input; green lines, results using 5 bins; black lines show results using full-offset traces; and blue lines are true values. The RMS error plots show a general progression of increasing accuracy as the number of bins increases. However, it is not a simple linear trend, as certain bin sizes appear much more effective than others: five bins seem to work better than three, although three bins still perform very well.

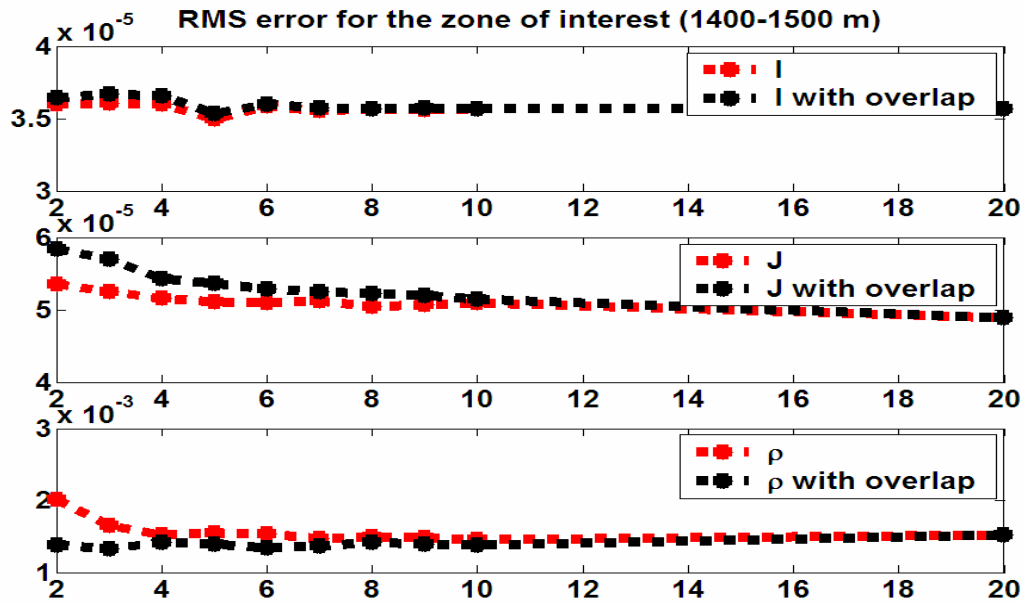


FIG. 22. The RMS-error plots of inversion results using different binning sizes. The input log is shown in Figure 11.

At present, we do not know whether these results are particular to the geometry and lithology of our example or are more general. We suspect that the effectiveness of a particular binning scheme will depend upon the behaviour with offset of  $R_{pp}$  and  $R_{ps}$ . If these functions vary linearly across the bin, then the average reflection coefficient over the bin is well approximated by the value of the coefficient at the bin centre. In this case, the binning scheme should succeed. It does seem safe to conclude that there is little need to maintain all offset traces without binning and a small number of bins will give excellent results. Since offset binning leads to very efficient prestack migration schemes, there is a strong economic incentive for binning.

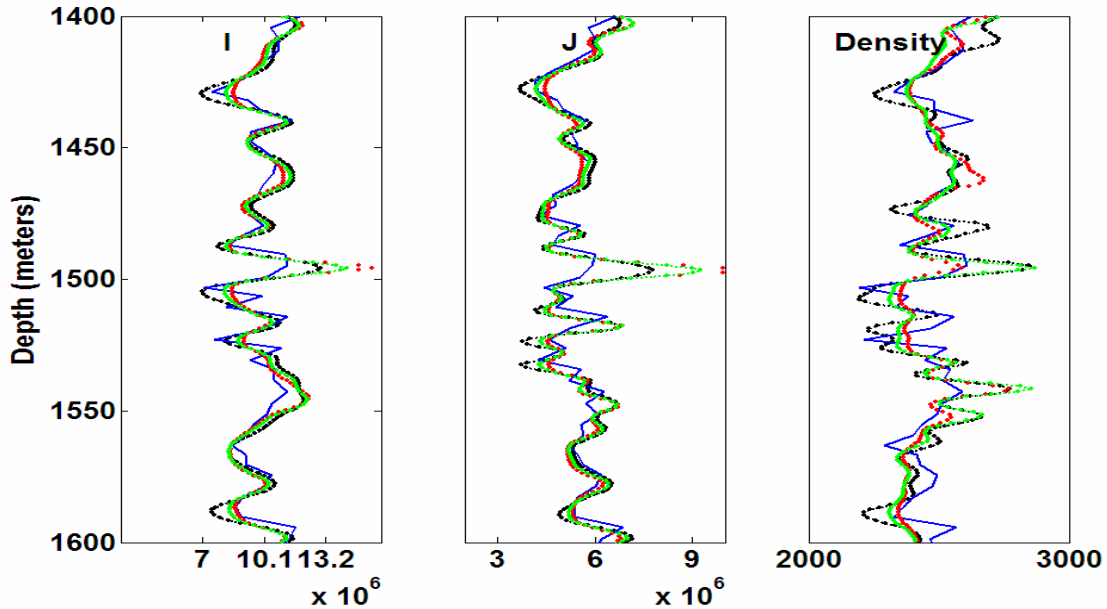


FIG. 23. P- and S-wave impedance, and density estimations from 3-parameter joint inversion with 3 bins, 5 bins with no overlap, full traces with no binning, and the actual values.

## CONCLUSIONS

This paper developed and demonstrated a 3-parameter AVO joint inversion utilizing the SVD method. The algorithm was successfully demonstrated on synthetic data. P- and S-wave impedance, and density were successfully estimated from noisy datasets even when the density was uncorrelated with the P-wave velocity. We discussed the advantages of using the SVD method over the normal least-squares method for inverting singular or near-singular matrixes. The 3-parameter inversion results are more accurate compared to the 2-parameter joint inversion and 3-parameter PP- and PS-only inversions. We examined the input binning-size effect on inversion results. We concluded there is little need to maintain all offset traces without binning and that a small number of bins give excellent results.

## ACKNOWLEDGEMENTS

The authors would like to thank CREWES industrial sponsors and the Canadian government funding agencies, NSERC and MITACS, for funding this research. Our appreciation to EnCana and UNOCAL for providing the logs, and especial thanks to Brooke Berard for proofreading the text.

## REFERENCES

- Ferguson R. J., and Margrave, G. F., 1996, A simple algorithm for band-pass impedance inversion, CREWES Research Report, **8**, 1–10.
- Henley, D. C., Margrave, G. F., and Zhang, H., 2002, Preparing input data for joint PP/PS inversion, CREWES Research Report, **14**, 1–11.
- Jackson, D. D., 1972, Interpretation of inaccurate, insufficient and inconsistent data: Geophys. J. R. Astr. Soc., **28**, 97–109.

- Larsen, J. A., 1999, AVO inversion by simultaneous PP and PS inversion: M.Sc. Thesis, University of Calgary.
- Lay, D. C., 1997, *Linear Algebra and its Applications*, 2<sup>nd</sup> Ed.: Addison-Wesley.
- Zhang, H., and Margrave, G. F., 2003, Joint PP-PS inversion at Pikes Peak oilfield, Saskatchewan: CREWES Research Report, **15**, 1–12.
- Mahmoudian, F., and Margrave, G. F., 2003, AVO inversion of multi-component data for P- and S-impedance: CREWES Research Report, **15**, 1–34.
- Smith, G. C., and Gidlow, P.M., 1987, Weighted stacking for rock property estimation and detection of gas: *Geophysical Prospecting*, **35**, 993–1014.
- Stewart, R. R., 1990, Joint P and P-SV inversion: CREWES Research Report, **2**, 112–115.